ACCOUNTS
of chemical research

The Energetics of Supported Metal Nanoparticles: Relationships to Sintering Rates and Catalytic Activity

CHARLES T. CAMPBELL*
Department of Chemistry, University of Washington, Seattle, Washington 98195-1700, United States

RECEIVED ON JANUARY 3, 2013

CONSPECTUS

Transition metal nanoparticles on the surfaces of oxide and carbon support materials form the basis for most solid catalysts and electrocatalysts, and have important industrial applications such as fuel production, fuels, and pollution prevention. In this Account, I review my laboratory group's research toward the basic understanding of the effects of particle size and support material on catalytic properties. I focus on studies of well-defined model metal nanoparticle catalysts supported on single-crystalline oxide surfaces. My group structurally characterized such catalysts using a variety of ultrahigh vacuum surface science techniques. We then measured the energies of metal atoms in these supported nanoparticles, using adsorption calorimetry tools that we developed. These metal adsorption energies increase with increasing size of the nanoparticles, until their diameter exceeds about 6 nm. Below 6 nm, the nature of the oxide support surface reaches also greatly affects the metal adsorption energies. Using both adsorption calorimetry and temperature programmed desorption (TPD), we measured the energy of adsorbed catalytic intermediates on metal nanoparticles supported on single crystal oxide surfaces, as a function of particle size. The studies reveal correlations between a number of characteristics. These include the size- and support-dependent energies of metal surface atoms in supported metal nanoparticles, their rates of sintering, how strongly they bind small adsorbates, and their catalytic activity. The data are consistent with the following model: the more weakly the surface metal atom is attached to the nanomaterial, the more strongly it binds small adsorbates. Its strength of attachment to the nanomaterial is dominated by the number of metal–metal bonds which bind it there, but also by the strength of metal/oxide interfacial bonding. This same combination of bond strengths controls sintering rates as well: the less stable a surface metal atom is in the nanomaterial, the greater is the thermodynamic driving force for it to sinter, and the faster is its sintering rate. These correlations provide key insights into how and why specific structural properties of catalyst nanomaterials dictate their catalytic properties. For example, they explain why supported Au catalysts must contain Au nanoparticles smaller than about 6 nm to have high activity for combustion and selective oxidation reactions. Only below about 6 nm are the Au atoms so weakly attached to the catalyst that they bind oxygen sufficiently strongly to enable the activation of O_2. By characterizing this interplay between industrially important rates (of net catalytic reactions, of elementary steps in the catalytic mechanism, and of sintering) and their thermodynamic driving forces, we can achieve a deeper fundamental understanding of supported metal nanoparticle catalysts. This understanding may facilitate development of better catalytic nanomaterials for clean, sustainable energy technologies.

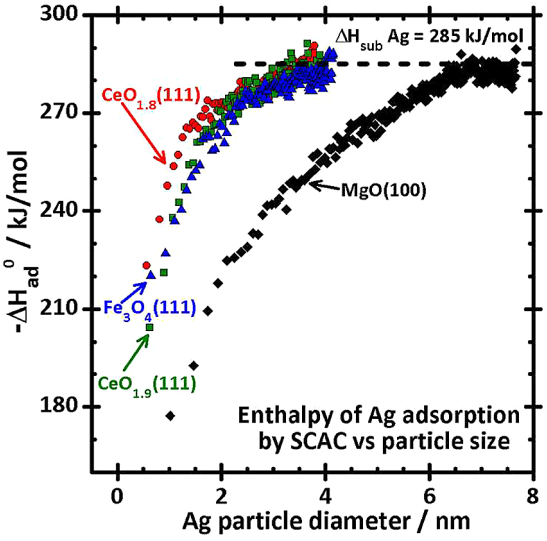

1. Introduction

Metal nanoparticles supported on oxide and carbon surfaces form the basis for many catalysts and electrocatalysts of importance in energy technologies, pollution prevention and environmental cleanup. The catalytic activity per surface metal atom and selectivity can vary strongly with particle size when below about 6 nm, and they also depend strongly on the support material.[1−4] Furthermore, under catalytic reaction conditions, metal nanoparticles can sinter (i.e., convert to fewer, larger particles), resulting in loss of

Published on the Web 04/22/2013 www.pubs.acs.org/accounts
10.1021/ar3003514

activity and selectivity, thus decreasing the efficiency and cleanliness of the process. The rate of such sintering depends very strongly on particle size and support material.[5−7] To understand how to make better catalyst materials, there is great interest in knowing how the rates of catalytic reactions and of sintering depend upon nanoparticle size and upon the support material.

To clarify these structure−reactivity relationships in such catalysts and their sintering kinetics, a number of researchers have adopted a model catalysts approach whereby structurally better-defined samples are prepared by vapor deposition of the metal onto single-crystal oxide surfaces.[1,5,8,9] The deposited metal atoms generally nucleate small particles, whose size and number density can be controlled by the amount of deposited metal and temperature. The aim is to correlate the metal's chemisorption, catalytic, sintering, and/or electronic properties with the lateral diameter, the thickness and composition of the nanoparticles, and the surface composition and structure of the support material upon which they sit.

Our group added a unique element to this approach, whereby we measure the energies of the metal atoms in these well-defined metal nanoparticles supported on clean surfaces of single-crystal oxides using metal adsorption calorimetry, a method we developed that is not available anywhere else in the world. We found that these energetics correlate with the chemical and catalytic reactivity of these nanoparticles and with their sintering rates. Here, we review those results, and discuss the interplay between the stability of metal atoms which form the catalytic sites, the strength with which they bind adsorbates, and their sintering rates.

2. Metal Atom Stability within Metal Nanoparticles Varies Strongly with Particle Size

We have calorimetrically measured the heats of adsorption of different metal atoms (Ag, Cu, Ca, Li, Pb) onto single crystal oxide surfaces as model supports for nanoparticle catalysts, including MgO(100), CeO_2(111), and Fe_3O_4(111).[10−24] Example heat versus coverage data are shown in Figure 1. Heats are always expressed here as the standard enthalpy of adsorption, ΔH_{ad}^0, at the stated temperature. ("Standard" means 1 bar gas pressure, with ΔH_{ad} independent of pressure below that.)

When late transition metals are vapor deposited onto single crystal surfaces of the materials used as supports for metal catalysts, they typically grow as 3D clusters rather than wetting the surface.[5] The number of clusters per unit area grows initially with coverage, but usually saturates after a few percent of a monolayer (ML), and thereafter they grow in size at nearly fixed number density until the particles grow together and coallesce.[5,25] For these cases, the heat of metal adsorption typically starts out low for tiny clusters and increases with coverage as the cluster size grows. This is the case for all the curves in Figure 1 except Ca/MgO(100). For the other system, this saturation cluster density is expected to have been reached already after the first pulse with the fluxes used (~0.02 ML/pulse).

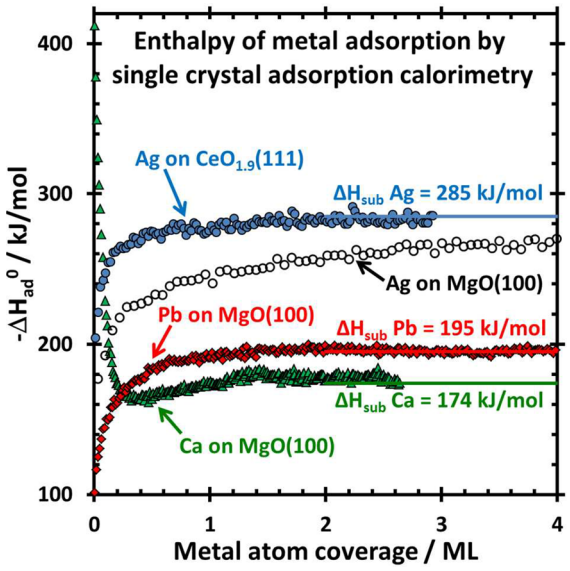

FIGURE 1. Example heats of adsorption versus coverage data for metals on single-crystal oxides as measured by calorimetry at 300 K. Data are shown for Pb, Ag, and Ca on MgO(100) and Ag on CeO_2(111) (with 5% oxygen vacancies in the XPS probe depth). Data from refs 14, 16, 19, and 23. One ML equals the number of oxygen ions per unit area in the topmost atomic plane (1.12×10^{15} cm^{-2} for MgO(100) and 7.9×10^{14} cm^{-2} for CeO_2(111)). Horizontal lines mark the bulk heats of sublimation. Adapted with permission from ref 43. Copyright 2013 American Chemical Society.

The initial heats of adsorption for Pb, Ag, and Cu on MgO(100) at 300 K were found to increase with their bulk sublimation enthalpies.[10] Their initial sticking probabilities at 300 K and saturation number densities of metal particles also were found to increase with the magnitude of their initial heats of adsorption.[10] This supports a transient mobile precursor model for adsorption,[10] which is consistent with DFT-calculated energetics for transition metal adatoms at terrace sites and the small magnitudes of their diffusion barriers.[26] It is also consistent with classic mechanistic/kinetic models developed by Venables to explain electron microscopy observations of cluster nucleation and growth.[25] The results all support the conclusion that isolated adatoms of metals like Ag, Cu, and Pd on oxides like MgO(100) are highly mobile at room temperature, and diffuse rapidly from site to site across the oxide until finding a growing metal cluster.

Heat of adsorption versus coverage data of the type shown in Figure 1 can be integrated to obtain the adhesion

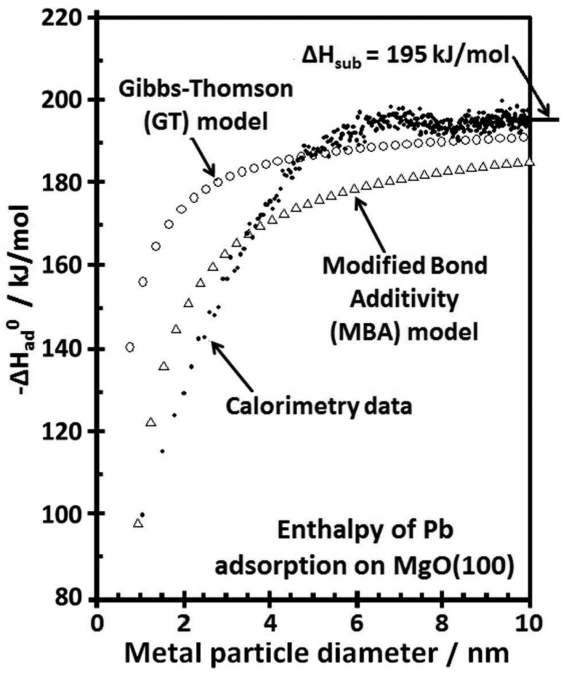

FIGURE 2. Heat of adsorption of Pb onto Pb nanopartcles on MgO(100) versus average Pb particle diameter. Also shown is the Gibbs–Thomson model of eq 2, which assumes that the surface energy is the bulk value, independent of particle size. This is seen to fit the experimental data very poorly below 4 nm. In contrast, the modified bond additivity (MBA) model, which is also shown (see details in text), is a much better estimate for the experimental data. Adapted with permission from ref 11. Copyright 2002 American Association for the Advancement of Science.

energy between a multilayer metal film and the underlying oxide surface.[27] We analyzed these adhesion energies for Ag, Cu, and Pb on MgO(100) together with the adhesion energy from Pd/MgO(100) from contact angle measurements and found that the adhesion energy correlates with the sum of the magnitudes of the metal's bulk sublimation enthalpy plus the heat of formation of the bulk oxide of the metal (per mole of metal atoms).[10] This suggests that local chemical bonds, both metal–oxygen and covalent metal–Mg, dominate the interfacial bonding. The morphology of metal clusters (2D vs 3D) grown by vapor deposition on TiO_2(110) and measured by scanning tunneling microscopy (STM) also correlate with a combination of the metal's bulk sublimation enthalpy and the heat of formation of the bulk oxide of that metal.[28] Several other models have been offered to explain trends in metal/oxide adhesion energies with respect to the choice of the metal and of the oxide.[29,30]

For metals that grow as 3D particles, it is often possible to estimate the average particle size versus coverage from spectroscopic or other surface measurements. In these cases, it is possible to replot the heat of adsorption versus coverage data of the type shown in Figure 1 instead as heat of adsorption versus average metal particle size. We did this first for the case of Pb on MgO(100),[11] as shown in Figure 2. Here the Pb and MgO Auger electron spectroscopy (AES) peak intensities versus coverage were analyzed assuming a fixed number density of Pb particles (N_{sat}), independent of Pb coverage,[16] as noted above to be typical. This gave a value for N_{sat} of 8×10^{11} particles/cm^2. Dividing the Pb coverage (atoms/cm^2) by N_{sat} (particles/cm^2) gives the average number of Pb atoms per particle versus coverage, which can be combined with the bulk density of Pb (atoms/cm^3) to give the average particle volume (V) at each coverage. Assuming a hemispherical shape, this volume then gives the average Pb particle diameter at that coverage: $d = (6V/\pi)^{1/3}$. Dividing the average coverage during the first pulse (1.2×10^{13} atoms/cm^2) by N_{sat} gives that these clusters contain ~15 Pb atoms on average during the first pulse's heat measurement at 300 K.[16] For the qualitatively similar Ag on MgO(100) data of Figure 1, this number is ~12 atoms.[14]

The Gibbs–Thompson (GT) relation states that the chemical potential (partial molar free energy) of a metal atom in a particle of radius R, $\mu(R)$, differs from that in the bulk, $\mu(\infty)$, by

$$\mu(R) - \mu(\infty) = 2\gamma\Omega/R \qquad (1)$$

where γ is the surface free energy of the bulk metal and Ω is the volume per atom in the bulk solid.[31] Neglecting entropy differences, this gives that

$$\Delta H_{sub} + \Delta H_{ad}(R) = \mu(R) - \mu(\infty) = 2\gamma\Omega/R \qquad (2)$$

where ΔH_{sub} is the bulk heat of sublimation. As shown in Figure 2, this model qualitatively fits the data, but for small particles, this model severely overestimates the stability of Pb in small Pb particles, by ~60 kJ/mol at 2 nm diameter. This is because the average coordination number of the surface atoms decreases for small particles. In the large-particle limit for the most stable (111) face of FCC metals, each added metal atom makes six metal–metal bonds when it adsorbs. However, it makes only three such bonds (on average) when it adds to a metal trimer. Thus, the surface energy is not really a constant, but instead must actually increase substantially as the diameter decreases below ~6 nm. For this same reason, more open or stepped crystal facets of metals (where the metal atoms have fewer nearest neighbor) have higher surface energies.[32]

A modified pairwise bond-additivity (MBA) model shown in Figure 2 reproduces this strong dependence of adsorption enthalpy on cluster size reasonably well. This model is described in detail elsewhere.[6,11] In it, the energies of discrete,

pyramidal clusters were calculated assuming that all metal−metal bond energies equal their bulk value (32.5 kJ/mol for Pb, which is 1/6 of the sublimation energy of the bulk solid[33]), with their effective hemispherical diameters calculated from their volumes. We interpret this good agreement as indicating that the dominant effect at play here is rather trivial: when metal atoms add to smaller metal particles, they make fewer bonds (on average). More complex electronic size effects turn on below ~2 nm.[34] The experimental heats in Figure 2 are higher than the GT model above 5 nm, probably due a +5% calorimetry calibration error. The GT model fits the data better than the MBA model above 5 nm, even if the heats are scaled by 95% to account for this. However, the differences there (<10 kJ/mol) are small compared to the errors of ~30−60 kJ/mol in the GT model in the 1−3 nm range.

We also measured the heat of adsorption for Pb on MgO(100) at 190 K and found similar behavior to that in Figures 1 and 2, with an initial heat of adsorption that was almost identical as at 300 K, but with a much larger saturation cluster density at 190 K, thus giving much smaller particles at most coverages. Because of this, the heat of adsorption were also much smaller than at 300 K for most coverages, until the heat reached its bulk value.[17]

Supported metal catalysts often sinter or coarsen with time during use, starting from a collection of many small, highly dispersed nanoparticles and eventually converting to their thermodynamically preferred state: fewer, larger particles.[5,7,31,35−38] To model the kinetics of sintering on the basis of atomistic mechanisms, the GT relation (eq 2) has generally been assumed.[31,35,39] As noted above, the GT model overestimates particle stability in the size range of most interest in this respect. Thus, we found that the MBA model provides a much more accurate kinetic model for sintering for Au on TiO_2(110), with physically more reasonable parameters, and it helps explain previous anomalies in sintering kinetics.[6,11] It also helps explain the size-focusing observed during colloidal nanoparticle growth from liquid solutions.[40]

3. Ag Atom Adsorption Enthalpies and Ag Nanoparticle Stabilities Depend Strongly on the Nature of the Oxide Surface

Our calorimetric adsorption enthalpies of Ag atoms onto several different oxides show that the choice of support can greatly alter the stability of nanoparticles of the same metal and size, as summarized in Figure 3. The measured heats of adsorption of Ag gas atoms are plotted here versus the average Ag particle diameter to which it adds for four oxides:

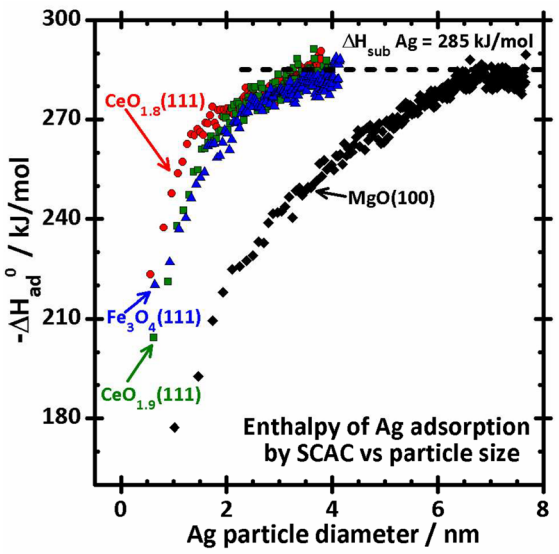

FIGURE 3. Heat of Ag atom adsorption during experiments where Ag is vapor deposited onto oxide surfaces at 300 K where Ag atoms transiently adsorb on clean parts of the oxide surface but quickly diffuse across the surface and adds to growing Ag particles on the surface. Plotted here is the measured heat of Ag atom adsorption versus the Ag particle diameter to which it adds (i.e., the average Ag particle size at the Ag coverage corresponding to that heat value). Data are shown for four different surfaces: Fe_3O_4(111) thin film and two CeO_2(111) thin films with different extents of surface reduction (x = ~0.1 and 0.2 in CeO_{2-x}), all grown on Pt(111) to 4 or 5 nm thickness, and a 4 nm thick MgO(100) film grown on Mo(100). The data for Fe_3O_4(111) are from ref 24 and those for CeO_2(111) and MgO(100) are from ref 22. Adapted with permission from ref 24. Copyright 2011 Royal Society of Chemistry.

MgO(100), two slightly reduced CeO_2(111) surfaces, and Fe_3O_4(111). We used the above approach to convert from Ag coverage to effective particle diameter. The Ag film morphology was measured versus Ag coverage using a combination of AES and He^+ low-energy ion scattering spectroscopy (ISS). The AES and ISS data were well fitted by assuming the Ag particles have the shape of hemispherical caps, with a fixed number density that is independent of Ag coverage after the first 2% of a ML,[14,22] with saturation Ag particle densities (N) of 2.5−4 × 10^{12} particles/cm^2. The reduced CeO_{2-x} stoichiometries here refer to the surface only, as measured by XPS. For the less reduced $CeO_{1.9}$(111) surface, most of the oxygen vacancies are thought to reside at step edges.[22]

Figure 3 shows that the heat of adsorption increases rapidly with Ag particle size (coverage) on all these oxides, but reaches a saturation value for large silver particles which is indistinguishable from the bulk heat of Ag sublimation (285 kJ/mol[33]). Like Figure 2, the increase in heat with particle size in these curves is dominated by the effect of particle size on the number of metal−metal bonds per atom.

TABLE 1. Calorimetrically Measured Adhesion Energies of Ag Nanoparticles to MgO(100), Two Reduced CeO_{2-x}(111) Surfaces and Fe_3O_4(111), and the Initial Heats of Ag Adsorption ($\Delta H_{ad,init}^0$) for the First Pulse (~0.03 monolayer) of Ag Gas at 300 K[a]

substrate surface	Ag adhesion energy/J/m^2	Ag coverage/atoms/cm^2	Ag particle size/nm	$\Delta H_{ad,init}^0$/ kJ/mol
MgO(100)	0.3 ± 0.3[14]	9.6×10^{15}	6.6	176
$CeO_{1.9}$(111)	2.3 ± 0.3	2.8×10^{15}	3.6	200
$CeO_{1.8}$(111)	2.5 ± 0.3	2.8×10^{15}	3.6	220
Fe_3O_4(111)	2.5 ± 0.3	2.8×10^{15}	3.6	220
Ag(solid)	2.44[14]	∞[b]	∞[b]	285[c]

[a]Also listed are the Ag particle size and Ag coverage used to get the adhesion energy. The adhesion energy for Ag on Ag (i.e., twice the surface energy of bulk Ag(solid)) is also given. Reproduced with permission from ref 43. Copyright 2013 American Chemical Society. [b]Bulk Ag(solid): the high-coverage/large-particle limit. [c]Heat of sublimation of bulk Ag.

Note that the Ag atoms bind much more strongly to sub-4 nm Ag particles on the Fe_3O_4(111) and reduced CeO_2(111) surfaces than to the same size particles on MgO(100). For all these surfaces, the metal particles nucleate mainly at steps,[5,22,41] but the particles are big enough in the 1.5–4 nm range that most of the metal atoms at the metal/oxide interface are *not* directly bonding to oxide step atoms, but instead to terrace atoms, as shown also by STM images of Ag particles grown on this same type of CeO_2(111) film in ref 41. Thus, these heat data prove that the bonding of Ag particles is stronger to Fe_3O_4(111) and reduced CeO_2(111) than for MgO(100), even at terrace sites.

Figure 3 also shows that Ag binds ~15 kJ/mol more strongly to small Ag clusters (<1.5 nm) when they are on the more reduced $CeO_{1.8}$(111) surface than on $CeO_{1.9}$(111). This increase in stability with surface vacancy concentration is consistent with DFT predictions.[42]

One can extract the adhesion energy from heat of metal adsorption versus coverage curves such as those in Figure 1.[27] We applied this to the data for Ag on the four different oxide surfaces in Figure 3, and the resulting adhesion energies are summarized in Table 1.

As seen, the adhesion energies of Ag nanoparticles to CeO_2(111) and Fe_3O_4(111) are much larger than those to MgO(100). It also increases with the extent of reduction of the CeO_2. These adhesion energies correlate with the initial adsorption energy of Ag, as expected, since both should reflect the strength of Ag-oxide bonding. Surface hydroxyls increase the initial heat of adsorption for Cu on MgO(100).[18]

4. Variations in Metal Atom Stability with Particle Size and Support Are Crucial for Understanding the Rates at Which Catalysts Deactivate by Sintering

Figure 4 shows the same data as Figure 3, but replotted as the enthalpy of a metal atom after it adds to a particle relative to its enthalpy in bulk Ag (or the partial molar enthalpy) versus particle size. This plot directly reflects the thermodynamic driving force for nanoparticle sintering: The atoms in the particles want to move down the curves to the lowest-energy state (i.e., the large-particle limit). As seen, Ag atoms are 30–70 kJ/mol more stable in Ag nanoparticles smaller than ~4 nm (1000 atoms) when those particles are attached to CeO_{2-x}(111) and Fe_3O_4(111) surfaces than to MgO(100) surfaces. This difference gets smaller for larger particles, and essentially disappears by ~6 nm, where the energy of the added metal atom reaches the stability of bulk Ag(solid) even on MgO(100). Clearly, sintering should be slower for small Ag particles on CeO_2 and Fe_3O_4(111) surfaces than on MgO(100), if the rate accelerates with the thermodynamic driving force as usual in atomic-level chemical processes. Since Au nanoparticles are very active for several catalytic reactions when 3 nm, but inactive above 6 nm[3], the ability to inhibit sintering in this range of particular sizes is crucial.

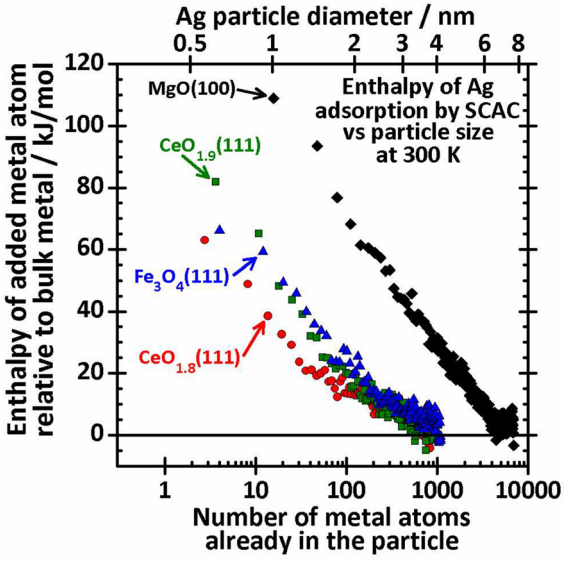

FIGURE 4. Partial molar enthalpy of Ag atoms in Ag nanoparticles (i.e., the enthalpy of the last Ag atom to be added to the particle, relative to bulk solid Ag) versus the average Ag particle size for Ag adsorption on different oxide surfaces. Used with permission from ref 43. Copyright 2013 American Chemical Society.

We have developed rate equations based on microkinetic models of sintering mechanisms.[6,11,40] Sintering occurs by two mechanisms: (1) Ostwald ripening or (2) particle diffusion/coalescence. In Ostwald ripening, individual metal atoms leave a metal particle and diffuse around on the support surface until they join another metal particle. Since the energy per atom is lower in larger particles (Figure 4), this leads to the growth of larger particles at the expense of smaller ones, who decrease in size and eventually disappear. Diffusing monomers can be stabilized by complexation with coadsorbed gases to accelerate sintering. In particle diffusion/coalescence, whole metal particles diffuse across the support until they come into contact with another particle and coalesce. Independent of which mechanism dominates, our rate equations for sintering show that the enthalpy in Figure 4 strongly affects the sintering rate, as a negative contribution to the apparent activation energy.[6,11,40] For example, for Ostwald ripening under common conditions, the rate of change of a particle's diameter (D) is given by

$$dD/dt = (K/D)e^{-E_{tot}/kT}(e^{H(D^*)/kT} - e^{H(D)/kT}) \qquad (3)$$

where $H(D)$ is the y-axis enthalpy value in Figure 4 and D^* is the diameter of particles with $dD/dt = 0$. Particles smaller than D^* get smaller (i.e., dD/dT is negative), and those larger than D^* grow. Here E_{tot} is the metal's bulk sublimation enthalpy minus the adsorption energy of a monomer on the support plus the diffusion activation energy of a metal monomer atom on the support, k is Boltzmann's constant, and K is the prefactor for a metal atom to detach from a large particle and become a monomer on the support, times a geometric constant. If sintering is instead dominated by particle diffusion/coalescence, its rate is proportional to $e^{H(D)/kT}$.[39]

Given that sintering rates increase with $e^{H(D)/kT}$, the data in Figure 4 show that sintering should be much slower on CeO_2 and Fe_3O_4(111) surfaces than on MgO(100). This is consistent with observations that ceria offers a more sinter-resistant support for late transition metals than many other oxides.[44,45] This is also consistent with our STM and noncontact atomic force microscopy (nc-AFM) results (Figures 5 and 6), showing that Pd nanoparticles sinter more rapidly on α-Al_2O_3(0001)[46] than on CeO_2(111). These STM data are for strongly reduced CeO_{2-x}(111).

The validity of eq 3 was verified by using it to successfully simulate experimentally measured sintering rates.[6,11,40] The sintering kinetics were measured using temperature-programmed low-energy ion scattering spectroscopy (TP-LEIS), which measures the very broad range of apparent activation energies in a single heating. These results showed that the apparent activation energy for sintering increases dramatically with particle size from 1 to 6 nm, due to the effect of particle size on the chemical potential of its metal atoms (i.e., upon $H(D)$ in Figure 4D).[6,11,40] Since the support material has a large effect on $H(D)$ (Figure 4), one can expect huge effects of support on sintering rates.

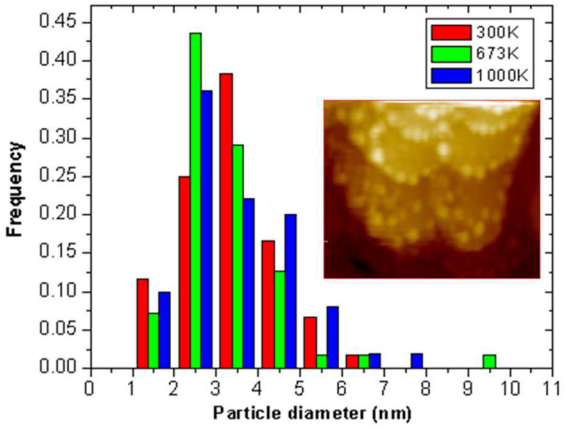

FIGURE 5. Size distributions of Pd nanoparticles on a reduced CeO_2-(111) surface as prepared at 300 K and after annealing briefly to 673 and 1000 K in UHV, measured by STM. Inset shows a typical STM image (75 nm x 44 nm). Unpublished data, taken by Dr. Simon Penner under direction of this author.

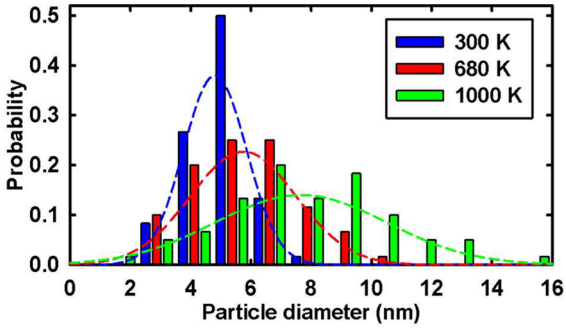

FIGURE 6. Apparent size distributions of Pd nanoparticles on an α-Al_2O_3(0001) surface as prepared at 300 K and after annealing briefly to 680 and 1000 K in UHV, measured by nc-AFM. The initial size distribution is biased to larger sizes than reality due to the inability of nc-AFM to detect most particles smaller than ~3 nm. Reproduced with permission from ref 46. Copyright American Institute of Physics 2005.

5. Variations in Metal Atom Stability with Particle Size and Support Affect the Stability of Adsorbed Catalytic Intermediates

We now explain why the relative energy of a metal atom in a catalytic surface is expected to correlate with the reactivity of that metal center. First, the strength with which atom A bonds to another atom B decreases with the number of bonds A already has to other atoms, or with atom A's total

TABLE 2. Activation Energies for Desorption of Oxygen Adatoms as $O_{2,gas}$ from Au Nanoparticles of Increasing Size (average thickness) on TiO_2(110), from refs 52 and 54 (see erratum, ref 53); Values from ref 55 for Specific Sites on Bulk Au(211), Which Has Short Au(111) Terraces Separating Periodic Steps, Are Also Shown for Comparison

average Au nanoparticle thickness (atomic layers)	activation energy for desorption (kJ per mol O_2)	oxygen adatom's desorption peak temperature (K)
1.3	190	740
2.3	165	645
6	139	545
bulk Au(211) step site	142	540
bulk Au(111) terrace site	138	515−530

bond order to other atoms. For example, the C−C bond energy decreases from 970 to 730 to 380 kJ/mol as the number of H atoms on each of these two C atoms increases from 1 (in ethyne) to 2 (ethane) to 3 (ethane), while the total bond order to each of the two C atoms remains fixed at 4. Similarly, a common trend in organometallic chemistry is that the reactivity of a metal center increases as its degree of coordinative unsaturation increases. The simple bond energy-bond order conservation (BEBO) model[47−49] quantified this qualitative trend and extended it to estimating activation barriers. We extended this qualitative picture to metal atoms in catalytic surfaces, arguing that the more weakly a metal atom is bound to the surface of the catalyst material, the more strongly that metal atom is expected to covalently chemisorb small molecules.[50] This is consistent with the well-known trend that low-coordination metal atoms at steps on metal surfaces bind small molecules more strongly than do more stable metal atoms in higher-coordination environments such as in close-packed terraces. Conversely, when that same metal atom resides in a monolayer supported on some other metal to which it binds more strongly than to itself, as, for example in Pd monolayers on Mo(100) or Ta(110), it binds small molecules more weakly.[51]

Since metal atoms are bound more weakly to the smallest metal nanoparticles than to large metal particles (Figures 3 and 4), and have lower coordination number there, one expects metal atoms in the smallest metal particles to bind adsorbed catalytic reaction intermediates most strongly. As summarized in Table 2, this is certainly the case for O adatoms on Au nanoparticles on TiO_2(110). Here, analysis of their TPD peak temperatures for desorption as gaseous O_2 using simple Redhead analysis gave desorption activation energies that are ∼50 kJ/mol larger from the smallest Au particles, implying that O adatoms are at least 25 kJ/mol more stable on the smallest Au particles than on bulk Au.[52,53]

In general, we found that small metal nanoparticles on oxide supports, especially when only 1 atom thick, bind small adsorbates more strongly than large particles or bulk metal crystals.[5] This can have a dramatic effect in catalysis, and has been proposed to explain why small Au nanoparticles can activate O_2 for oxidation reactions.[52] Note that Au nanoparticles are only catalytically active when below 7 nm diameter.[3] This is the same size range where Ag atoms begin to have markedly lower stability than on bulk Ag surfaces (Figures 3 and 4). Thus, metal atom energetics are clearly reflected in both chemisorption bond strengths and catalytic activity.

This bond energy-bond order conservation concept, combined with Figure 3 or 4, also predicts that particle size effects on chemisorption bond strengths and catalytic activity will depend strongly on the support material. That is, for a given particle size below 6 nm, metal atoms are much less stable on a "weak" support like MgO(100) than on "strong" supports like CeO_2(111) and Fe_3O_4(111) (Figures 3 and 4). Thus they will bind adsorbates more strongly. They should also reach the large-particle limit in their chemisorption and catalytic properties at much smaller particle sizes when on "strong" supports like CeO_2(111) and Fe_3O_4(111) than "weak" support like MgO(100). This was proposed to partially explain heats of adsorption for CO on Pd on Fe_3O_4(111).[24]

The author gratefully acknowledges his present and former students and postdocs, whose superb data and publications made this review of their combined contributions possible, Jason Sellers for preparing some of the figures/tables, and support by DOE-OBES Grant #DE-FG02-96ER14630.

BIOGRAPHICAL INFORMATION

Charles T. Campbell is the B. Seymour Rabinovitch Endowed Chair in Chemistry at the University of Washington. He received his B. S. in Chemical Engineering (1975) and his Ph.D. in Physical Chemistry (1979, under J. M. White) from the University of Texas at Austin, and then did postdoctoral research in Germany under Gerhard Ertl (2007 Nobel Prize Winner). He is the author of over 270 publications on surface chemistry, catalysis, and biosensing. He is Editor-in-Chief of *Surface Science Reports* and was Editor-in-Chief of *Surface Science* for 11 years before that. He is an elected Fellow of both the American Chemical Society (ACS) and the American Association for the Advancement of Science. He received the Arthur W. Adamson Award of the ACS and the ACS Award for Colloid or Surface Chemistry, the Gerhard Ertl Lecture Award, the Ipatieff Lectureship at Northwestern University, and an Alexander von Humboldt Senior Research Award. He served as Chair, Chair-Elect, Vice-Chair, and Treasurer of the Colloid and Surface Chemistry Division of the ACS.

FOOTNOTES

*E-mail: campbell@chem.washington.edu.
The authors declare no competing financial interest.

REFERENCES

1 Goodman, D. W. Model Studies in Catalysis Using Surface Science Probes. *Chem. Rev.* **1995**, *95*, 523–536.

2 Haruta, M. Catalysis of gold nanoparticles deposited on metal oxides. *CATTECH* **2002**, *6*, 102–115.

3 Valden, M.; Lai, X.; Goodman, D. W. Onset of catalytic activity of gold clusters on titania with the appearance of nonmetallic properties. *Science* **1998**, *281*, 1647–1650.

4 Rodriguez, J. A.; Liu, P.; Wang, X.; Wen, W.; Hanson, J.; Hrbek, J.; Perez, M.; Evans, J. Water-gas shift activity of Cu surfaces and Cu nanoparticles supported on metal oxides. *Catal. Today* **2009**, *143*, 45–50.

5 Campbell, C. T. Ultrathin Metal Films on Oxide Surfaces: Structural, Electronic and Chemisorptive Properties. *Surf. Sci. Rep.* **1997**, *227*, 1–111.

6 Parker, S. C.; Campbell, C. T. Kinetic model for sintering of supported metal particles with improved size-dependent energetics and applications to Au on TiO_2(110). *Phys. Rev. B* **2007**, *75*, 035430.

7 Bartholomew, C. H. Sintering and redispersion of supported metals: perspectives from the literature of the past decade. In *Catalyst Deactivation*; Bartholomew, C. H., Fuentes, G. A., Eds.; Elsevier Science B.V.: Amsterdam, 1997; p 585.

8 Henry, C. R.; Chapon, C.; Giorgio, S.; Goyhenex, C. Size effects in heterogeneous catalysis: A surface science approach. In *Chemisorption and Reactivity on Supported Clusters and Thin Films*; Lambert, R. M., Pacchioni, G., Eds.; Kluwer Academic Publishers: Amsterdam, 1997; p 117.

9 Bäumer, M.; Freund, H.-J. Metal deposits on well-ordered oxide films. *Prog. Surf. Sci.* **1999**, *61*, 127–198.

10 Campbell, C. T.; Starr, D. E. Metal Adsorption and Adhesion Energies on MgO(100). *J. Am. Chem. Soc.* **2002**, *124*, 9212–9218.

11 Campbell, C. T.; Parker, S. C.; Starr, D. E. The effect of size-dependent nanoparticle energetics on catalyst sintering. *Science* **2002**, *298*, 811–814.

12 Campbell, C. T.; Lytken, O. Experimental measurements of the energetics of surface reactions. *Surf. Sci.* **2009**, *603*, 1365–1372.

13 Ranney, J. T.; Starr, D. E.; Musgrove, J. E.; Bald, D. J.; Campbell, C. T. A Microcalorimetric Study of the Heat of Adsorption of Copper on Well-Defined Oxide Thin Film Surfaces: MgO(100), p(2 $\times$ 1)-Oxide on Mo(100), and Disordered W Oxide. *Faraday Discuss.* **1999**, *114*, 195–208.

14 Larsen, J. H.; Ranney, J. T.; Starr, D. E.; Musgrove, J. E.; Campbell, C. T. Adsorption energetics for Ag on MgO(100). *Phys. Rev.* **2001**, *B 63*, 195410.

15 Larsen, J. H.; Starr, D. E.; Campbell, C. T. Enthalpies of Adsorption of Metal Atoms on Single-Crystalline Surfaces by Microcalorimetry. *J. Chem. Thermodyn.* **2001**, *33*, 333–345.

16 Starr, D. E.; Bald, D. J.; Musgrove, J.; Ranney, J.; Campbell, C. T. Microcalorimetric measurements of the heat of adsorption of Pb on well-defined oxides: MgO(100) and p(2 $\times$ 1)-oxide on Mo(100). *J. Chem. Phys.* **2001**, *114*, 3752–3764.

17 Starr, D. E.; Campbell, C. T. Low-temperature adsorption microcalorimetry: Pb/MgO(100). *J. Phys. Chem. B* **2001**, *105*, 3776–3782.

18 Starr, D. E.; Diaz, S. F.; Musgrove, J. E.; Ranney, J. T.; Bald, D. J.; Nelen, L.; Ihm, H.; Campbell, C. T. Heat of Adsorption of Cu and Pb on Hydroxyl-covered MgO(100). *Surf. Sci.* **2002**, *515*, 13–20.

19 Zhu, J.; Farmer, J. A.; Ruzycki, N.; Xu, L.; Campbell, C. T.; Henkelman, G. Calcium adsorption on MgO(100): Energetics, structure, and role of defects. *J. Am. Chem. Soc.* **2008**, *130*, 2314–2322.

20 Farmer, J. A.; Ruzycki, N.; Zhu, J. F.; Campbell, C. T. Lithium adsorption on MgO(100) and its defects: Charge transfer, structure, and energetics. *Phys. Rev. B* **2009**, *80*, 035418.

21 Farmer, J. A.; Ruzycki, N.; Zhu, J.; Xu, L.; Campbell, C. T.; Henkelman, G. Defect Sites and their Distributions on MgO(100) by Li and Ca Adsorption Calorimetry. *J. Am. Chem. Soc.* **2009**, *131*, 3098–3103.

22 Farmer, J. A.; Campbell, C. T. Ceria Maintains Smaller Metal Catalyst Particles by Strong Metal-Support Bonding. *Science* **2010**, *329*, 933–936.

23 Farmer, J. A.; Baricuatro, J. H.; Campbell, C. T. Ag Adsorption on Reduced CeO_2(111) Thin Films. *J. Phys. Chem. C* **2010**, *114*, 17166–17172.

24 Campbell, C. T.; Sharp, J. C.; Yao, Y. X.; Karp, E. M.; Silbaugh, T. L. Insights into Catalysis by Gold Nanoparticles and their Support Effects through Surface Science Studies of Model Catalysts. *Faraday Discuss.* **2011**, *152*, 227–239.

25 Venables, J. A. *Introduction to Surface and Thin Film Processes*; Cambridge University Press: Cambridge, 2000; 372 pages, pp 144−180.

26 Xu, L.; Henkelman, G.; Campbell, C. T.; Jonsson, H. Kinetic Monte Carlo simulations of Pd deposition and island growth on MgO(100). *Surf. Sci.* **2007**, *601*, 3133–3142.

27 Stuckless, J. T.; Starr, D. E.; Bald, D. J.; Campbell, C. T. Metal Adsorption Calorimetry and Adhesion Energies on Clean Single-Crystal Surfaces. *J. Chem. Phys.* **1997**, *107*, 5547–5553.

28 Hu, M.; Noda, S.; Komiyama, H. A new insight into the growth mode of metals on TiO2(110). *Surf. Sci.* **2002**, *513*, 530–538.

29 Chatain, D.; Coudurier, L.; Eustathopoulos, N. Wetting and Interfacial Bounding in Ionocovalent Oxide-Liquid Metal Sustems. *Rev. Phys. Appl.* **1988**, *23*, 1055–1064.

30 Didier, F.; Jupille, J. The van der Waals Contribution to the Adhesion Energy at Metal-Oxide Interfaces. *Surf. Sci.* **1994**, *314*, 378–384.

31 Wynblatt, P.; Gjostein, N. A. Particle growth in supported model catalysts: I. Theory. *Acta Metall.* **1976**, *24*, 1165–1174.

32 Galanakis, I.; Papanikolaou, N.; Dederichs, P. H. Applicability of broken-bond rule to the surface energy of the fcc metals. *Surf. Sci.* **2002**, *511*, 1–12.

33 Lide, D. R. *CRC Handbook of Chemistry and Physics (Internet Version)*, 88th ed.; CRC Press/Taylor and Francis: Boca Raton, FL, 2008.

34 Li, L.; Larsen, A. H.; Romero, N. A.; Morozov, V. A.; Glinsvad, C.; Abild-Pedersen, F.; Greeley, J.; Jacobsen, K. W.; Norskov, J. K. Investigation of Catalytic Finite-Size-Effects of Platinum Metal Clusters. *J. Phys. Chem Lett.* **2013**, *4*, 222–226.

35 Wynblatt, P.; Gjostein, N. A. Supported metal crystallites. In *Progress in Solid State Chemistry*; McCaldin, J. O., Somorjai, G. A., Eds.; Pergamon: Oxford, 1975; Vol. *9*, p 21.

36 Ruckenstein, E.; Dadyburjor, D. B. Sintering and redispersion in supported metal catalysts. *Rev. Chem. Eng.* **1983**, *1*, 251–282.

37 Fuentes, G. A.; Salinas-Rodriguez, E. Asymptotic behavior during sintering of supported catalysts. In *Catalyst Deactivation*; Bartholomew, C. H., Fuentes, G. A., Eds.; Elsevier Science: Amsterdam, 1997; p 573.

38 Sehested, J. Sintering of nickel steam-reforming catalysts. *J. Catal.* **2003**, *217*, 417–426.

39 Jak, M. J.; Konstapel, C.; Kreuningen, A. v.; Crost, J.; Verhoeven, J.; Frenken, J. W. The influence of substrate defects on the growth rate of Pd nanoparticles on TiO2(110). *Surf. Sci.* **2001**, *474*, 28–36.

40 Parker, S. C.; Campbell, C. T. Reactivity and sintering kinetics of Au/TiO2(110) model catalysts: particle size effects. *Top. Catal.* **2007**, *44*, 3–13.

41 Luches, P.; Pagliuca, F.; Valeri, S.; Illas, F.; Preda, G.; Pacchioni, G. Nature of Ag Islands and Nanoparticles on the CeO_2(111) Surface. *J. Phys. Chem. C* **2012**, *116*, 1122–1132.

42 Wang, J. H.; Liu, M. L.; Lin, M. C. Oxygen reduction reactions in the SOFC cathode of Ag/CeO2. *Solid State Ionics* **2006**, *177*, 939–947.

43 Campbell, C. T.; Sellers, J. R. V. Enthalpies and Entropies of Adsorption on Well-Defined Oxide Surfaces: Experimental Measurements. *Chem. Rev.* DOI: 10.1021/cr300329s.

44 Kalakkad, D.; Datye, A. K.; Robota, H. Interaction of platinum and ceria probed by transmission electron-microscopy and catalytic reactivity. *Appl. Catal., B* **1992**, *1*, 191–219.

45 Schwartz, J. M.; Schmidt, L. D. Microstructures of Pt-Ce and Rh-Ce particles on alumina and silica. *J. Catal.* **1992**, *138*, 283–293.

46 Tait, S. L.; Ngo, L. T.; Yu, Q. M.; Fain, S. C.; Campbell, C. T. Growth and sintering of Pd clusters on α-Al_2O_3(0001). *J. Chem. Phys.* **2005**, *122*, 064712.

47 Johnston, H. S.; Parr, C. Activation Energies from Bond Energies 0.1. Hydrogen Transfer Reactions. *J. Am. Chem. Soc.* **1963**, *85*, 2544–2551.

48 Weinberg, W. H.; Merrill, R. P. Crystal-Field Surface Orbital - Bond-Energy Bond-Order (CFSO-BEBO) Model for Chemisorption - Application to Hydrogen Adsorption on a Pt(111) Surface. *Surf. Sci.* **1972**, *33*, 493–515.

49 Weinberg, W. H. Bone-Energy Bond-Order (BEBO) Model of Chemisorption. *J. Vac. Sci. Technol.* **1973**, *10*, 89–94.

50 Campbell, C. T.; Grant, A. W.; Starr, D. E.; Parker, S. C.; Bondzie, V. E. Model Oxide-Supported Metal Catalysts: Energetics, Particle Thicknesses, Chemisorption and Catalytic Properties. *Top. Catal.* **2000**, *14*, 43–51.

51 Heitzinger, J. M.; Geghard, S. C.; Koel, B. E. Chemisorption of CO on Ultrathin Films of Pd on Mo(100). *Surf. Sci.* **1992**, *275*, 209–222.

52 Bondzie, V.; Parker, S. C.; Campbell, C. T. The Kinetics of CO Oxidation by Adsorbed Oxygen on Well-Defined Gold Particles on TiO_2(110). *Catal. Lett.* **1999**, *63*, 143–151.

53 Bondzie, V.; Parker, S. C.; Campbell, C. T. Erratum to ref **52**. *Catal. Lett.* **2011**, *141*, 1721–1721.

54 Bondzie, V.; Parker, S. C.; Campbell, C. T. Oxygen Adsorption on Well-Defined Gold Particles on TiO_2(110). *J. Vac. Sci. Technol.* **1999**, *A17*, 1717–1720.

55 Kim, J.; Samano, E.; Koel, B. E. Oxygen adsorption and oxidation reactions on Au(211) surfaces: Exposures using O_2 at high pressures and ozone(O_3) in UHV. *Surf. Sci.* **2006**, *600*, 4622–4632.